DOI 10.1007/s10553-024-01728-4
Chemistry and Technology of Fuels and Oils, Vol. 60, No.3, July, 2024 (Russian Original No.3, May – June, 2024)

INNOVATIVE TECHNOLOGIES OF OIL AND GAS

STUDYING THE ACCUMULATION CHARACTERISTICS OF CRUDE OIL IN AN OIL FORMATION IN THE ASPECT OF PREDICTING THE EFFECTIVENESS OF CRUDE OIL EXPLORATION

Yande Zhao[1] ✉, Xiao Hui[2], Zhongyi Zhang[2], Mingyi Yang[2], Anxiang Luo[2], Qing Guo[1]

The development of tight oil sandstones in the Extension Formation in the southwestern Ordos Basin and the mode of crude oil migration is a hotspot. A large number of geochemical experiments and computational methods were used to systematically study the crude oil transport characteristics of the Yanchang Formation in the Huaqing area. The results show that four typical types of inclusions are developed in the Yanchang Formation: inclusions in quartz fissures, inclusions in quartz colluvium and large rims, inclusions in calcareous colluvium, and inclusions in sodium feldspar. There are two peaks in the homogenization temperature of the inclusions: 80-100°C and 120-130°C. The Chang 6 and Chang 8 reservoirs in the Huaqing area have experienced the process of densification while forming reservoirs, and the physical properties of the sand body reservoirs during the maximum hydrocarbon discharge period are good, which is an effective channel for oil and gas transportation. The minimum oil column heights for oil and gas transportation in Chang 6 and Chang 8 Members are 7.48m and 15.68m, respectively. Proximity vertical transportation is an important mode of crude oil transportation and aggregation in the Yanchang oil group in the Huaqing area. The physical properties of crude oil in Huaqing area are good, showing low density, low viscosity, low freezing point and good fluidity. The hydrocarbon source rocks of the Chang 7 Member were transported under excess pressure and buoyancy along channels such as cheese root networks, connected sands and microfractures, and thus large composite lithologic reservoirs were formed in the Chang 6 and Chang 8 Members.

Keywords: crude oil, hydrocarbon aggregation, inclusions, accumulation characteristics.

1. Introduction

China is rich in low-permeability and ultra-low-permeability oil and gas resources, and the proven geological reserves of low-permeability oil fields account for about 35% of all proven geological reserves [1-3]. In recent years, the oilfields discovered and not put into development in China are also mainly low-permeability and ultra-low-permeability oilfields represented by Changqing oilfield [4-6]. With China's increasing demand for oil, the recoverable reserves of easy-to-exploit medium- and high-permeability

[1] BaiLie School of Petroleum Engineering, Lanzhou City University, Lanzhou, China; [2] Exploration & Development Research Institute of PetroChina Changqing Oilfield Company, Xi'an, China. *Corresponding author: Yande Zhao ✉. E-mail: zydlzcu@163.com.* Translated from *Khimiya i Tekhnologiya Topliv i Masel*, No. 3, pp. 159–164, May – June, 2024.

oilfields are gradually declining, and low- and ultra-low-permeability oilfields, including tight oilfields, will contribute more and more to oil and gas production [7, 8].

The Chang 8-Chang 6 reservoir of Yanchang Formation in the Ordos Basin Basin is generally a low-permeability reservoir, but in the planar distribution, the reservoirs on different sedimentary zones have different reservoir physical properties and pore structures. Delta front edge due to the proximity of the littoral zone, the lake wave scouring, elution effect is strong, the heterogeneous base content is low, so the delta front edge of the phase zone primary intergranular pore preservation is better, the local existence of high permeability zones, that is, high-quality reservoirs [9-11]. Turbiditic sandstones in the Semi-Deep Lake-Deep Lake area have fine grain size, high filler content, poor physical properties, and relatively low crude oil yields because they are the product of redeposition from the delta front [12, 13].

Huaqing area is located in the central area of the lake basin of the Ordos Basin, and the main sparing system of low-permeability reservoirs and the mechanism and mode of hydrocarbon formation in this area are not well understood [14]. The existence of these problems restricts the effect of prediction and affects the effectiveness of crude oil exploration. In order to recognize the petroleum distribution pattern of Yanchang Formation in this area, it is urgent to study the petroleum channeling system and reservoir formation mechanism [15-17]. In this paper, a large number of geochemical experiments and computational methods were used to systematically study the crude oil transport characteristics of the Yanchang Formation in the Huaqing area. This study can provide a reference for efficient exploration of tight oil in the Yanchang Formation.

2. Geological background and methods

2.1. Geological background

The Huaqing area of the Ordos Basin is located in the sedimentary center of the lake basin. The Yanchang Formation in this area develops deep-water sandstone with large thickness and stable distribution, and the continuous thickness can reach hundreds of meters in local areas. Gravity flow deposits are predominantly developed in the central part of the lake basin in this region, which can be further classified into turbidity currents and debris flows. Turbidity is a kind of density flow mixed by sediment and water, which is a turbid fluid with high speed and turbulence at the bottom of the water body [18, 19]. Its density is greater than that of the surrounding liquid, and it takes advantage of this difference in density to move in a monolithic block along the slope under the force of gravity. The support mechanism for turbidity currents is provided by the upward partial force of turbulence within the fluid and keeps the sediment particles continuously suspended in the fluid. The turbidites in the study area are mainly composed of thin- to medium-thickly bedded pink-fine sandstones interbedded with gray-green and dark-gray mudstones and silty mudstones, with orthogranularity and multi-phase rhyolitic cyclones [20-22].

Debris flow is a mixture of water and clay and debris, with sand and gravel being carried by a matrix of water and clay support [23]. The mixture of clay and water is dense for normal water and thus more buoyant to debris particles, and the denser it is, the coarser the particles it supports and carries. The debris flow deposits found in the Huaqing area are associated with submarine landslide events, with high variability in thickness, sand and mud mixing and intense deformation. The sand body is mainly dominated by thick-bedded fine sandstone. Among them, the blocky fine sandstone sections are generally above 1m, and finally up to about 10m; parallel laminated sections are locally developed, and the thickness is generally below 0.1m [24, 25]. The siltstone and mudstone interbedding are rare and is characterized by the development of floating mud gravels, muddy debris and irregularly distributed slaty mudstone riprap.

2.2. Methods

Inclusions experiment. Homogenized temperature tests were carried out on 213 inclusions of the Yanchang Formation in the study area. The petrography of the inclusions was carried out using a Leica M165C stereomicroscope (magnification 7.3-120 times) and a Zeiss Imager A2m polarizing/fluorescence microscope (magnification 50-500 times). To determine the homogeneous temperature of the inclusions, a microscopic temperature measurement system consisting of a MDSG600 geological hot and cold stage produced by Linkam (UK) and a polarizing/fluorescence microscope Axioskop40 produced by Zeiss (Germany) was used.

Geochemical experiment. Geochemical experiments include testing of carbon isotopes and chemical components of crude oil. The EA-IRMS analysis system consists of the MAT 253Plus Gas Stable Isotope Mass Spectrometer, the Flash 2000 HT Elemental Analyzer, and the ConFlo IV interface. We carried out chloroform extracts of crude oil feeds, and separation of family fractions. Saturated and aromatic hydrocarbons were analyzed by chromatography-mass spectrometry on a Finnigan MAT TSQ-45 GC/MS system. Chromatographic conditions: SE-54 elastomeric fused silica capillary column (25 m long, 0.25 mm inner diameter) was used to increase the temperature from 100°C to 300°C at a ramp rate of 4°C/min, and the carrier gas was helium. Chromatography and mass spectrometry: An Agilent 6890 flexible fused-silica capillary column (25m long, inner diameter 0.25 mm) equipped with an Agilent 5975 mass spectrometry selective detector was used to analyze the saturated hydrocarbon and aromatic hydrocarbon fractions using an HP-5MS fused-silica column and an HP-5MS fused-silica column. Mass spectrometry: ionization energy of 70 V.

Calculation of resistance to oil and gas transportation. For the resistance to prevent the transport of oil and gas are capillary resistance, intermolecular adsorption force and oil and gas downward or downward direction to overcome the buoyancy of the oil and gas, and the most important resistance for the capillary force [26-27]. The capillary force depends on the interfacial tension between the two fluids, the capillary radius and the wettability of the medium, which can be expressed by the equation [28-30]:

$$P_c = 2\delta\cos\theta/r, \tag{1}$$

where P_c is capillary pressure, MPa; δ – interfacial tension, N/m; θ – wetting angle; r – capillary radius, m.

Under reservoir conditions, the capillary pressure is as Equation (2):

$$P_{cR} = 2\delta_{ow}\cos\theta_{ow}/r. \tag{2}$$

The capillary forces obtained from the piezomercury analysis were:

$$P_{cHg} = 2\delta_{Hg}\cos\theta_{Hg}/r. \tag{3}$$

Using Equation (2)/(3), we get $Pc_R / Pc_{Hg} = \delta_{ow}\cos\theta_{ow} / \delta_{Hg}\cos\theta_{Hg}$

That is:

$$P_{cR} = P_{cHg}\delta_{ow}\cos\theta_{ow} / \delta_{Hg}\cos\theta_{Hg}, \tag{4}$$

where, P_{cR} – capillary pressure in reservoir condition, MPa; P_{cHg} – capillary pressure obtained by mercury compression analysis, MPa; δ_{Hg} – interfacial tension of mercury-mercury vapor, 480 mN/m; δ_{ow} – interfacial tension of oil-water surface in reservoir condition, taking the value of 30 mN/m; θ_{ow} – oil-water wetting contact angle, 0°; θ_{Hg} – mercury-rock wetting contact angle, 140°.

Substituting the above parameters into Eq. (4), the capillary pressure under reservoir conditions is obtained as equation

$$P_{cR} = 0.3195P_{cHg}. \tag{5}$$

Using the above equation and the capillary pressure obtained by laboratory pressure mercury analysis, the capillary pressure can be derived under reservoir conditions.

Calculation of the dynamics of oil and gas transportation. Buoyancy is the primary motive force in secondary transport, but is only a secondary motive force in primary transport. This is partly due to the fact that the buoyancy force is small in the tiny microcapillary pores of the hydrocarbon source rock relative to the intermolecular forces between the hydrocarbons and the rock and the capillary resistance [31]; on the other hand, in the complex pore structure of hydrocarbon source rocks, it is also difficult for oil and gas to be connected to a sufficient length (height) to generate enough buoyancy for initial transportation. Therefore, in the initial transport generally less consideration of buoyancy, but in the hydrocarbon source rock localized larger capillary pores or tectonic pores in the role of buoyancy still exists, is still oil and gas in the free phase to the upward or upward direction of the direction of hydrocarbon drainage of a driving force [32-33].

The formula for buoyancy can be expressed in the equation

$$F_{cR} = (\rho_w - \rho_o)gZ_o. \tag{6}$$

where, F_{cR} – buoyancy force, N; Z_o – height of oil column, m; g-acceleration of gravity, g/m^2; ρ_w – density of formation water (subsurface); ρ_o – density of oil under formation conditions.

If hydrodynamic factors are not taken into account, in the secondary transportation of oil and gas, the buoyancy force is greater than the capillary resistance in order to contribute to the flow of oil and gas in the conduit layer. That is, there is as equation

$$F_{cR} > P_{cR} = 0.3195P_{cHg}. \quad (7)$$

From equations (6) and (7), the equation for the height of the oil column in the critical state can be obtained as equation

$$Z_o = 0.3195P_{cHg}/(\rho_w - \rho_o)g. \quad (8)$$

3. Results

3.1. Characterization of inclusions development

Inclusion thermometry analysis shows that four types of inclusions are developed in the Yanchang Formation in the study area: inclusions in quartz fissures (**Figure 1**), inclusions in quartz colluvium (Fig. 1b) and large rims (Fig. 1c), inclusions in calcareous colluvium, and inclusions in sodic feldspars (Fig. 1d). The colors of the inclusions were mainly colorless, gray-brown, and light yellow, and there were two peaks in the homogeneous temperature of the inclusions: 80-100°C and 120-130°C (**Figure 2**).

The homogeneous temperature of inclusions in quartz fissures and solution holes is 120 to 125°C, and there are even many inclusions with temperatures exceeding 150°C. Inclusions in quartz fissures and solution holes are produced in beads and isolates and generally do not show fluorescence. Weakly fluorescent inclusions in quartz fissures and their dissolution pores, fissures without cut-through plus large edges. The mean temperature of inclusions in quartz colluvium and large rims averages 104°C. The inclusions are fluorescent. These inclusions are fluorescent, and the various features indicate that the inclusions in the quartz fissures are inherited inclusions. Hydrocarbon inclusions were captured in the quartz plus size margin, suggesting that there was hydrocarbon transport during the formation of the plus size margin.

The homogeneous temperature distribution of the secondary inclusions in the calcareous collodion is from 91 to 117°C, with an average of 98.1°C. The secondary inclusions in the calcareous collodion fluoresce strongly. In order to further analyze the diagenetic evolution and diagenetic stage of Yanchang Formation, electron microprobe analysis was performed on the carbonate cement, which is mainly composed of calcium oxide and contains a small amount of iron oxide. Thus, the carbonate cements are mainly iron calcite and iron dolomite cements.

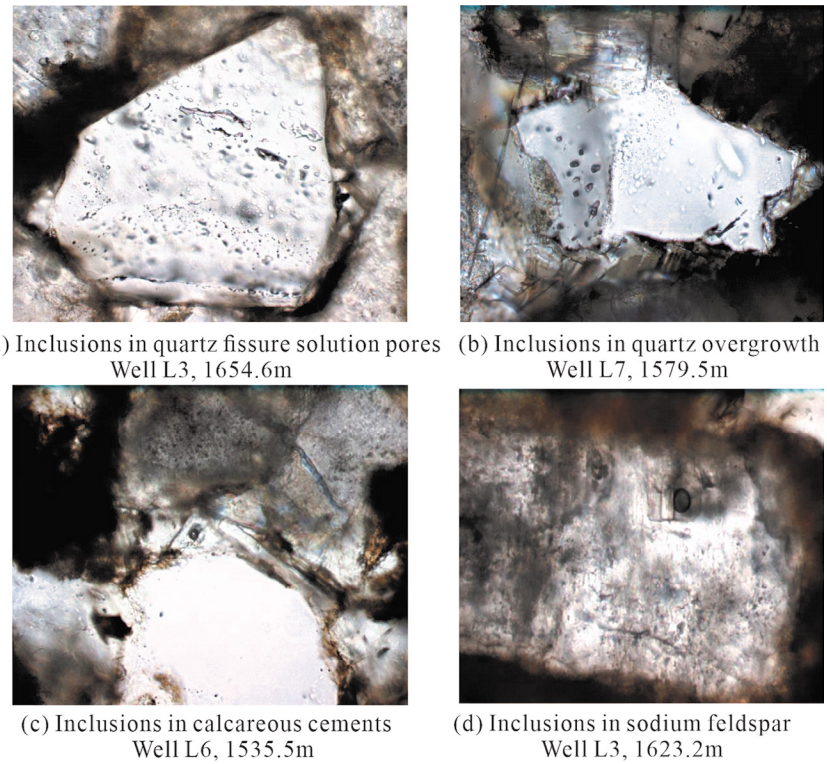

(a) Inclusions in quartz fissure solution pores Well L3, 1654.6m

(b) Inclusions in quartz overgrowth Well L7, 1579.5m

(c) Inclusions in calcareous cements Well L6, 1535.5m

(d) Inclusions in sodium feldspar Well L3, 1623.2m

Fig. 1. Types and developmental characteristics of inclusions in the Yanchang Formation, Huaqing area

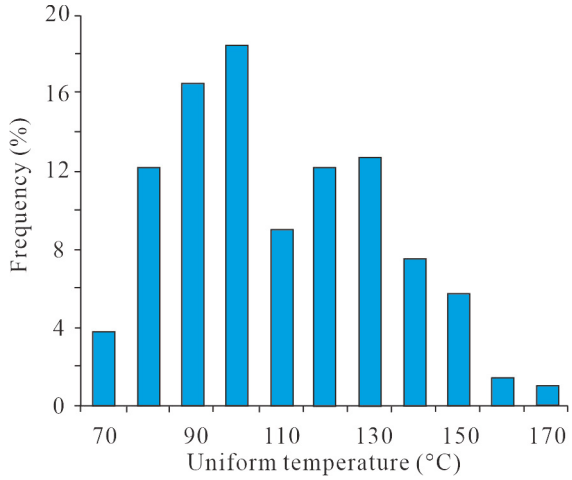

Fig. 2. Histogram of the distribution of the homogeneous temperature of the inclusions

The homogeneous temperature distribution of inclusions in sodium feldspar ranges from 91 to 117°C, with an average of 98.1°C, and the inclusions show strong fluorescence.

3.2. Effective corridors for oil and gas transportation

The Yanchang Formation undergoes feldspar dissolution and cementation during the middle diagenetic stage, and the mean temperature of inclusions captured during this stage averages 94°C. The inclusions in the Yanchang Formation are characterized by a high degree of feldspar dissolution and cementation. Dissolution of feldspars provides a source of material for siliceous cementation in the mesolithic stage, and the mean temperature of inclusions captured in the siliceous cementation stage averages 104°C. The iron-bearing carbonate cementation phase of the middle-late diagenetic stage changes from the preceding acidic environment to a weakly alkaline environment, and the mean temperature of inclusions captured during this period averages 98°C. The temperature of inclusions is the highest during the siliceous cementation period of the mesomorphic stage, and this period is in the stage of the maximum hydrocarbon discharge period, which is also generally recognized as the peak of hydrocarbon production and discharge. The quartz accretion is the diagenetic event of the period of maximum burial depth, and the porosity of that period can be approximated as equal to the present-day porosity plus the porosity converted by the diagenetic minerals from that period onward, i.e., the present-day porosity plus the porosity of the loss of Fe-dolomite and Fe-calcite Since illite is transformed from other clay minerals, the gain or loss of pore space during the transformation of illite is ignored here.

At present, the porosity of the Chang 6 and Chang 8 Formations is generally 10-13% and 7-11%, and the porosity of the late carbonate cementation losses is 5.5% and 5.2%. As a result, the porosity of the Chang 6 and Chang 8 Members of the maximum hydrocarbon generation and drainage stage is 16-20% and 12-16%, respectively. There is a good correlation between porosity and permeability in the Chang 6 and Chang 8 Members in the middle of the lake basin (**Figure 3**). A corresponding permeability value can be obtained for each recovered porosity value. Therefore, the paleo-permeability of the Chang 6 and Chang 8 Members during the maximum hydrocarbon discharge period is 2.5-13 mD and 2-10 mD, respectively.

From the above, it can be seen that the physical properties of the reservoir are relatively good during the maximum hydrocarbon discharge period, and the cementation of iron-containing carbonates is the decisive factor for the densification of the reservoir. The Chang 6 and Chang 8 reservoirs in the Huaqing area have experienced the process of densification while formation, and the physical properties of the sand reservoir during the maximum hydrocarbon discharge period are good, which can be used as an effective channel for oil and gas transportation.

3.3. Minimum column height for oil and gas transportation

The process of oil and gas aggregation and formation is the process of selecting the most favorable geological reservoir space under the action of driving force, and the nature of driving force determines the direction and intensity of oil and gas transportation.

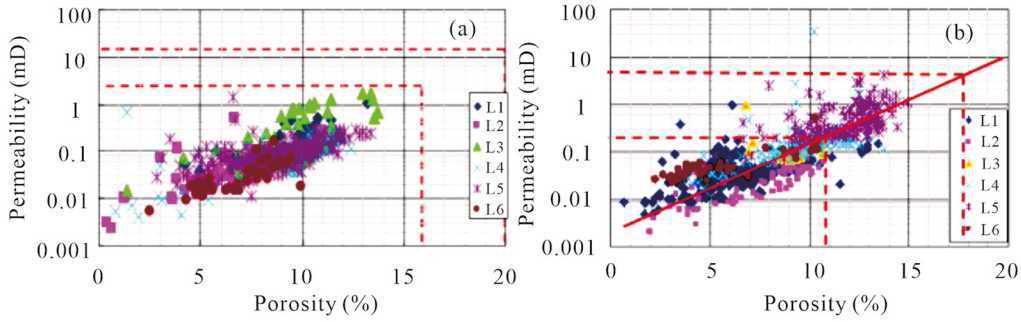

Fig. 3. Relationship between porosity and permeability in Chang 6 (a) and Chang 8 (b) Members of the study area

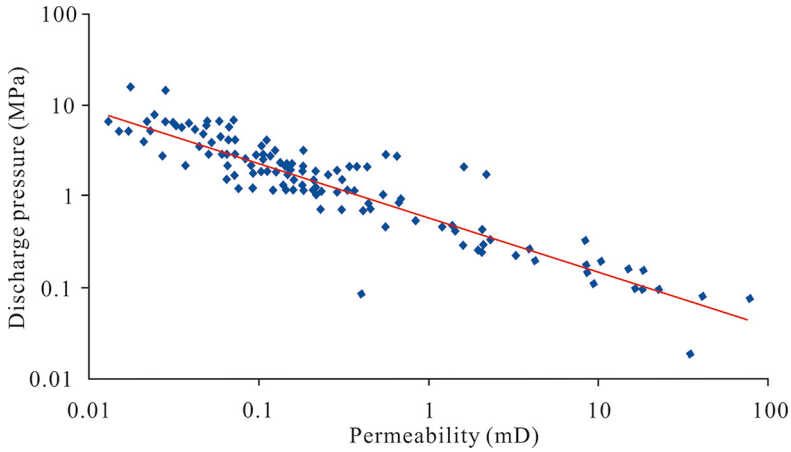

Fig. 4. Relationship between permeability and exhumation of samples from the Yanchang Formation

Therefore, analyzing the dynamics of oil and gas transport is an effective way to study oil and gas transport, aggregation and reservoir formation. In the secondary transportation of oil and gas, it is mostly carried out in the free phase state, and the main resistance of free-phase oil in the transportation process is capillary force.

Analysis of piezomercury data from 47 wells and 157 samples of different stratigraphic positions in the central part of the lake basin shows a double logarithmic linear relationship between discharge pressure and permeability (**Figure 4**). By recovering the physical properties of Chang 6-Chang 8 Members during the maximum hydrocarbon discharge period, the paleopermeability of Chang 6 Member during the maximum hydrocarbon discharge period ranged from 2.5 to 13 mD, the paleopermeability of Chang 7 Member ranged from 0.2 to 3 mD, and the paleopermeability of Chang 8 Member ranged from 2 to 10 mD. We take the upper limit value of permeability and substitute it into the equation of the fitting relationship between permeability and displacement pressure, we can derive the corresponding value of displacement pressure. Substituting the displacement pressure into Eq. (8), we can derive the minimum height of the oil column for buoyancy-driven oil and gas transportation in the state of the paleo-oil reservoirs, which is 7.48m in the Chang 6 Member and 15.68m in the Chang 8 Member.

4. Discussion

4.1. Carbon isotope analysis

Differences in fluid properties are determined by the different conditions of hydrocarbon formation and later changes in the reservoir. The density of crude oil in the Mesozoic Jurassic and Yanchang Formation Long 3 sections in the southern part of Tianhuan Depression is less than 0.88 g/cm^3, and the viscosity of crude oil is less than 100 mPa·s. The density of crude oil in the southern part of Tianhuan Depression is less than 0.88 g/cm^3. According to the crude oil evaluation standard, the physical

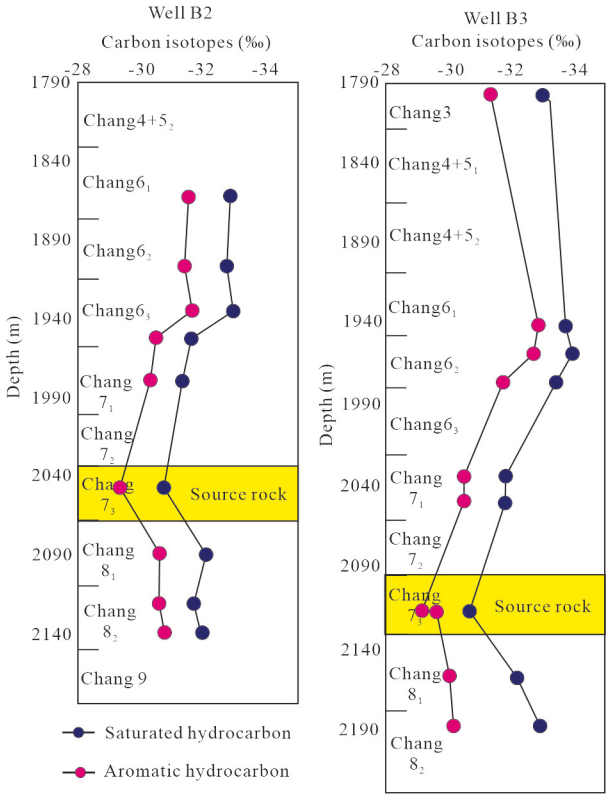

Fig. 5. Characteristics of longitudinal carbon isotope variations in typical wells in the Huaqing area

properties of crude oil in Huaqing area are good, showing the characteristics of low density, low viscosity, low freezing point, with good fluidity, and belongs to light oil.

The isotopic composition of petroleum depends on the nature of the original organic matter, the environment in which it was produced, and the degree of evolution. The stable carbon isotope compositions of petroleum of different genesis have large differences, but there are some compounds in crude oil and sedimentary organic matter that have large similarities in the basic carbon skeleton, and the carbon isotope composition characterization of crude oil is also an important means of studying the origin of hydrocarbons. W2 well saturated hydrocarbons: -32.16‰, aromatic hydrocarbons: -30.90‰; W3 well saturated hydrocarbons: -32.41‰, aromatic hydrocarbons: -30.85 ‰. Carbon isotopes become lighter from Chang 7 upward (Chang 6) to downward (Chang 8); saturated and aromatic hydrocarbon carbon isotopes have a similar pattern of change with depth (**Figure 5**).

4.2. Crude oil transport analysis based on nitrogenous compounds

The composition of these nitrogen-containing compounds in hydrocarbons changes regularly during oil and gas transportation. Shielded carbazoles continue to be relatively enriched, and exposed carbazoles continue to decrease. Based on the above pattern of change, the possible transportation path of oil and gas can be predicted in turn. With the increase of transportation distance, the content of such polar compounds in crude oil is decreasing, due to the different polarity of each compound, through the transportation fractionation, it will form a special form of distribution of polar compounds in oil after transportation.

Nitrogen in crude oil exists mainly in the form of aromatic heterocyclic compounds and amines, which are categorized into basic and non-basic nitrogen-containing compounds. Aromatic heterocyclic compounds are characterized by polarity: Non-basic nitrogen-containing compounds form hydrogen bonds through the nitrogen atoms on them, and basic nitrogen-containing compounds adsorb to the surrounding medium through ionic or hydrogen bonds. In the process of oil transportation, polar nitrogen-containing compounds interact with the surface of surrounding rocks (pores, cracks, etc.), and as the transportation distance increases, the content of such polar compounds in crude oil decreases, and the special distribution pattern of polar heterocyclic compounds in

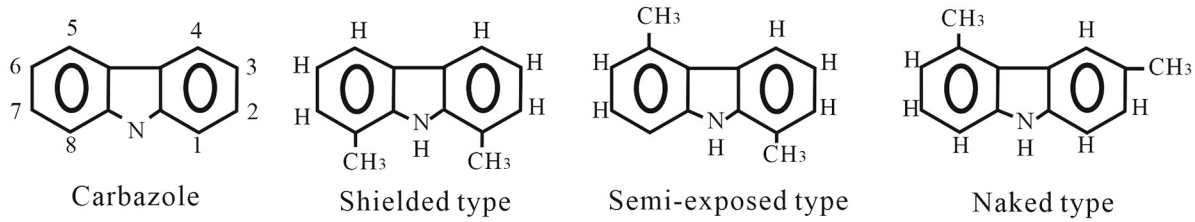

Fig. 6. Molecular structures of different polar carbazole endocompounds

crude oil after transportation is formed through fractionation. The reactivity of nitrogen-containing compounds will be attenuated if the nitrogen atom in carbazoles is partially or completely obscured by the alkyl group (**Figure 6**).

The two main types of nitrogen-containing compounds in crude oil are neutral pyrroles (including carbazoles, benzo carbazoles, etc.) and basic pyridines. An important property of nitrogen-containing heterocycles is their ability to interact with the formation surface or formation water through hydrogen bonding (pyrroles) and ionic or hydrogen bonding (pyridines). Different types of carbazole compounds in crude oil will undergo transport fractionation effect with the increase of crude oil transportation distance, so that the content of bare type compounds in crude oil will gradually decrease due to easy adsorption by the surrounding medium. The shielded type, on the other hand, has a gradually increasing content due to the small interaction with the surrounding medium. a) Carbazoles are more polar and decreasingly present in the extract as the distance traveled increases. b) Carbazoles have a slower rate of transport for the more polar molecules and a faster rate of transport for the less polar molecules: G3 (exposed) is more polar than G1 (shielded); C2-carbazole is more polar than C3-carbazole; trimethylcarbazole (C) [exposed] is more polar than trimethylcarbazole (A) [shielded]. c. compounds with small molecular scales are transported faster and compounds with large molecular scales are transported slower: Benzocarbazole has a larger molecular volume than alkylcarbazole; Benzocarbazole [c] (hemispherical) has a larger molecular volume than benzocarbazole [a] (linear). In summary, the transport effect on the composition of carbazole-containing nitrogen compounds is manifested in three main ways: the relative magnitude of the content of alkylcarbazoles versus alkylbenzocarbazoles, the relative magnitude of the content of nitrogen-shielded isomers versus nitrogen-exposed isomers, and the relative magnitude of the content of higher carbon-numbered homologs versus those of lower carbon-numbered homologs.

Crude oil carbazoles from various oil-bearing formations in the Huaqing area of the Ordos Basin are mainly composed of carbazole, C1-C3-carbazole, alkylcarbazole and benzocarbazole. And the content is dominated by dimethylcarbazole series compounds, followed by trimethylcarbazole series compounds, carbazole and benzocarbazole series compounds are relatively low. The relative abundance of carbazole isomers among themselves, especially the dimethylcarbazole shielded, partially shielded, and exposed compounds, changed as crude oil transport intensified. With the increase of 1,8-/2,7-dimethylcarbazole, the individual compound ratio parameters of C2- and C3-carbazoles characterizing shielded/exposed and shielded/partially shielded types increased accordingly, whereas the values of benzo[a]carbazole/benzo[c]carbazole decreased. The analysis also showed that the absolute concentration of nitrogen-containing compounds in crude oil had a good synergistic relationship with the ratio of shielded and exposed compounds, i.e., the absolute concentration of nitrogen-containing compounds decreased significantly with the increase of the 1,8-dimethylcarbazole/2,7-dimethylcarbazole value. Vertically, oil from the Triassic Yanchang Formation in the Huaqing area exhibits a bottom-to-top transport trend (**Figure 7**).

4.3. Analysis of crude oil transportation paths

In the process of oil transportation, pressure reduction is a prerequisite. The decrease of pressure inevitably makes the gas-oil ratio decrease gradually with the increase of transportation distance. The methane content remaining in the oil increases during lateral transportation due to the small adsorption force between the methane and the surrounding rock. During vertical transport, the low molecular hydrocarbon methane, which has a small molecular weight and is the most permeable, will escape preferentially, and both the gas-oil ratio and methane content will decrease.

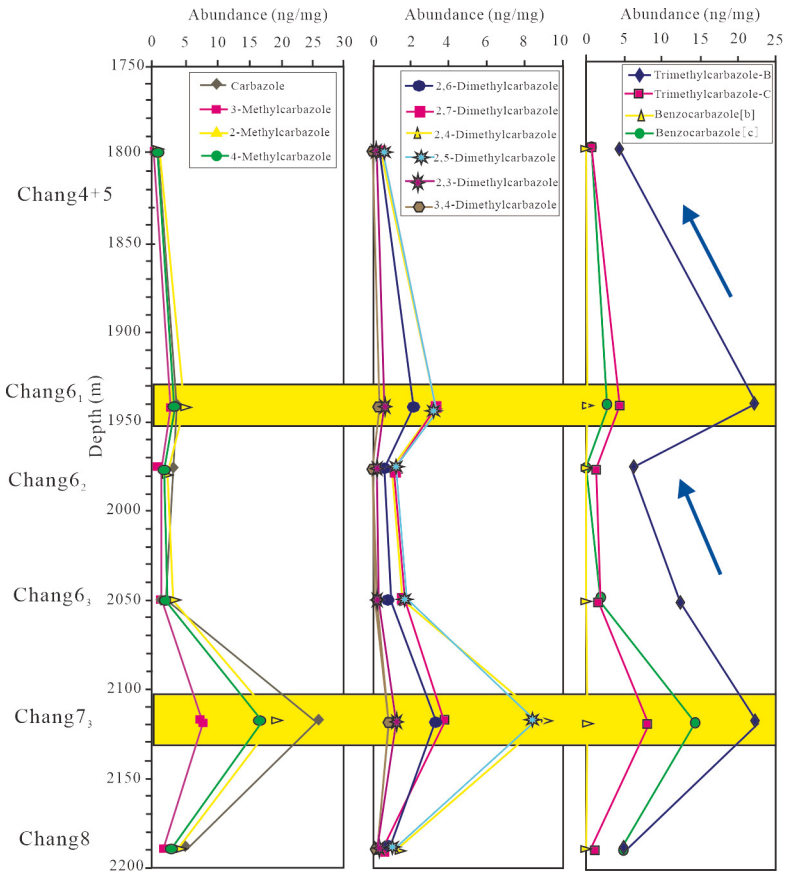

Fig. 7. Abundance characterization of nitrogenous compounds in well W61

According to the analysis of Kasimov's transport coefficient, the transport of petroleum in the Huaqing area shows that close vertical transport is an important way of oil and gas transportation and reservoir formation in this area (**Figure 8**). The Chang 7 Member hydrocarbon source rocks were transported under excess pressure and buoyancy along channels such as cheese root networks, connected sands and microfractures, and large composite lithologic reservoirs were formed in the Chang 6 and Chang 8 Members.

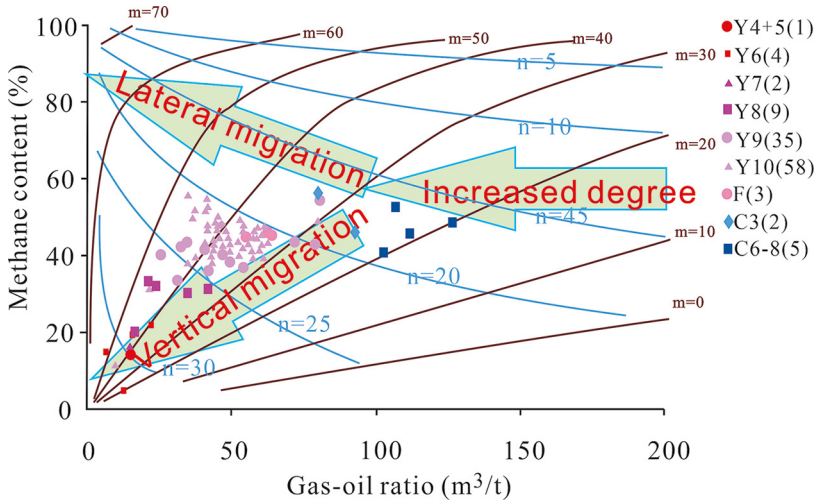

Fig. 8. Kasimov's line solving diagram for the Huaqing area

5. Conclusions

A large number of geochemical experiments and computational methods were used to systematically study the crude oil transport characteristics of the Yanchang Formation in the Huaqing area. Four typical types of inclusions are developed in the Yanchang Formation: inclusions in quartz fissures, inclusions in quartz colluvium and large rims, inclusions in calcareous colluvium, and inclusions in sodium feldspar. There are 2 peaks in the homogenization temperature of the inclusions: 80-100°C and 120-130°C.

The Chang 6 and Chang 8 reservoirs in the Huaqing area have experienced the process of densification while forming reservoirs, and the physical properties of the sand body reservoirs during the maximum hydrocarbon discharge period are good, which is an effective channel for oil and gas transportation. The minimum oil column heights for oil and gas transportation in Chang 6 and Chang 8 Members are 7.48m and 15.68m, respectively.

Proximity vertical transportation is an important mode of crude oil transportation and aggregation in the Yanchang oil group in the Huaqing area. The physical properties of crude oil in Huaqing area are good, showing low density, low viscosity, low freezing point and good fluidity. The hydrocarbon source rocks of the Chang 7 Member were transported under excess pressure and buoyancy along channels such as cheese root networks, connected sands and microfractures, and thus large composite lithologic reservoirs were formed in the Chang 6 and Chang 8 Members.

Acknowledgements

This work was financially supported by the Gansu Provincial Science and Technology Plan Project (No. 21JR7RA541), (Natural Science Foundation) (No. 22JR5RA546), the Prospective research project of CNPC (No.2021DJ2203), and the Education Technology Innovation Project in Gansu Province (Innovation Fund Project for University Teachers) (No.2023A-118).

REFERENCES

1. Liu Z., Shi B., Ge T., et al. Tight sandstone reservoir sensitivity and damage mechanism analysis: A case study from Ordos Basin, China and implications for reservoir damage prevention. *Energy Geoscience*, **2022**, 3(4), 394-416.

2. Chen Y., Wang Y., Guo M. Differential enrichment mechanism of organic matters in the marine-continental transitional shale in northeastern Ordos Basin, China: Control of sedimentary environments. *Journal of Natural Gas Science and Engineering*, **2020**, 83: 103625.

3. Yuan C.Z., Wang G., Li Q.Z., et al. Study on the origin and treatment of odor gas in heavy oil thermal recovery well site. *Chemical Engineering of Oil & Gas*, **2022**, 51(3), 145-150.

4. Baas J.H., Best J.L., Peakall J. Depositional processes, bedform development and hybrid bed formation in rapidly decelerated cohesive (mud-sand) sediment flows. *Sedimentology*, **2011**, 58(7), 1953-1987.

5. Cong S.N., Liu W.D., Guo Y., et al. Study on separation of crude oil component and interfacial activity based on liquid chromatography. *Chemical Engineering of Oil & Gas*, **2023**, 52(2), 76-80.

6. Zeng W.T., Zhang J.C., Ding W.L., et al. Fracture development in Paleozoic shale of Chongqing area (South China). Part one: Fracture characteristics and comparative analysis of main controlling factors. *Journal of Asian Earth Sciences*, **2013**, 75, 251-266.

7. Meiburg E., Kneller B. Turbidity currents and their deposits. *Annual Review of Fluid Mechanics*, **2010**, 42, 135-156.

8. Jazi S.D., Wells M.G. Dynamics of settling-riven convection beneath a sediment-laden buoyant overflow: Implications for the length-scale of deposition in lakes and the coastal ocean. *Sedimentology*, **2020**, 67(1), 699-720.

9. Jesús O., Jeannette W., Michael H.G. Recognition criteria for distinguishing between hemipelagic and pelagic mudrocks in the characterization of deep-water reservoir heterogeneity. *AAPG Bulletin*, **2013**, 97(10), 1785-1803.

10. Mulder T., Savoye B., Syvitski J. Numerical modelling of a mid-sized gravity flow: The 1979 Nice turbidity current (dynamics, processes, sediment budget and seafloor impact). *Sedimentology*, **1997**, 44(2), 305-326.

11. Mayall M., Kane I.A., McCaffrey W.D. Internal architecture, bedforms and geometry of turbidite channels. A conference held at the Geological Society, London, June 20-21st 2011. *Marine and Petroleum Geology*, **2013**, 41, 1-6.

12. Yin S., Wu Z. Geomechanical simulation of low-order fracture of tight sandstone. *Marine and Petroleum Geology*, **2020**, 100(34), 1-10.

13. Stow D., Johansson M. Deep-water massive sands: nature, origin and hydrocarbon implications. *Marine and Petroleum Geology*, **2000**, 17(2), 145-174.

14. Yin S., Dong L., Yang X., et al. Experimental investigation of the petrophysical properties, minerals, elements and pore structures in tight sandstones. *Journal of Natural Gas Science and Engineering*, **2020**, 76(1), 1-14.

15. Yadav K., Sircar A., Bist N. Carbon mitigation using CarbFix, CO_2 plume and carbon trading technologies. *Energy Geoscience*, **2023**, 4(1), 117-130.

16. Li L., Huang B., Li Y., et al. Multi-scale modeling of shale laminas and fracture networks in the Yanchang formation, Southern Ordos Basin, China. *Engineering Geology*, **2018**, 243, 231-240.

17. Lai J., Wang G.W., Wang Z.Y., et al. A review on pore structure characterization in tight sandstones. *Earth-Science Reviews*, **2018**, 177, 436-457.

18. Li J., Li H., Yang C., et al. Geological characteristics and controlling factors of deep shale gas enrichment of the Wufeng-Longmaxi Formation in the southern Sichuan Basin, China. *Lithosphere*, **2022**, 4737801.

19. Yin S., Tian T., Wu Z., et al. Developmental characteristics and distribution law of fractures in a tight sandstone reservoir in a low-amplitude tectonic zone, eastern Ordos Basin, China. *Geological Journal*, **2020**, 55, 1546-1562.

20. Kane I.A., Pontén A. Submarine transitional flow deposits in the Paleogene Gulf of Mexico. *Geology*, **2012**, 40(12), 1119-1122.

21. Katz B., Gao L., Little J., et al. Geology still matters-Unconventional petroleum system disappointments and failures. *Unconventional Resources*, **2021**, 1, 18-38.

22. Parsons J., Bush J., Syvitski J. Hyperpycnal plume formation from riverine outflows with small sediment concentrations. *Sedimentology*, **2001**, 48(2), 465-478.

23. Pattison S., Bruce A.R., Hoffman T.A. Evidence of across-helf transport of fine-grained sediments: Turbidite-filled shelf channels in the Campanian Aberdeen Member, Book Cliffs, Utah, USA. *Sedimentology*, **2007**, 54(5), 1033-1064.

24. Pritchard D., Gladstone C. Reversing buoyancy in turbidity currents: developing a hypothesis for flow transformation and for deposit facies and architecture. *Marine & Petroleum Geology*, **2009**, 26(10), 1997-2010.

25. Shanmugam G. New perspectives on deep-water sandstones: Implications. *Petroleum Exploration and Development*, **2013**, 40(3), 316-32.

26. Stevenson C.J. Peakall J. Effects of topography on lofting gravity flows: Implications for the deposition of deep-water massive sands. *Marine and Petroleum Geology*, **2010**, 27(7), 1366-1378.

27. Talling P.J., Paull C.K., Piper D.J. How are subaqueous sediment density flows triggered, what is their internal structure and how does it evolve? Direct observations from monitoring of active flows. *Earth-Science Reviews*, **2013**, 125, 244-287.

28. Talling P.J. On the triggers, resulting flow types and frequencies of subaqueous sediment density flows in different settings. *Marine Geology*, **2014**, 352, 155-182.

29. Yuan H., Yin S., Dong L., et al. Restoration of the pre-Jurassic paleogeomorphology and its control on hydrocarbon distribution in western Ordos Basin. *Energy Geoscience*, **2022**, 3(4), 485-494.

30. Zavala C., Arcuri M. Intrabasinal and extrabasinal turbidites: Origin and distinctive characteristics. *Sedimentary Geology*, **2016**, 337, 36-54.

31. Osinowo O., Abdulmumin Y., Faweya T. Analysis of high-resolution airborne-magnetic data for hydrocarbon generation and preservation potential evaluation of Yola sub-basins, northern Benue Trough, northeastern Nigeria. *Energy Geoscience*, **2023**, 4(1), 33-41.

32. Xiao Z., Ding W., Liu J., et al. A fracture identification method for low-permeability sandstone based on R/S analysis and the finite difference method: A case study from the Chang 6 reservoir in Huaqing oilfield, Ordos Basin. *Journal of Petroleum Science and Engineering*, **2019**, 174, 1169-1178.

33. Xie X., Heller P.L. U-Pb detrital zircon geochronology and its implications: The early Late Triassic Yanchang Formation, south Ordos Basin, China. *Journal of Asian Earth Sciences*, **2013**, 64, 86-98.